Structure-Guided Design of a Synthetic Mimic of an Endothelial Protein C Receptor-Binding PfEMP1 Protein

Natalie M. Barber,[a] Clinton K. Y. Lau,[a] Louise Turner,[b,d] Gareth Watson,[a] Susan Thrane,[b,d] John P. A. Lusingu,[c]
Thomas Lavstsen,[b,d] Matthew K. Higgins[a]

[a]Department of Biochemistry, University of Oxford, Oxford, United Kingdom

[b]Centre for Medical Parasitology, Department of Immunology & Microbiology, University of Copenhagen, Copenhagen, Denmark

[c]National Institute for Medical Research, Dar es Salaam, Tanzania

[d]Centre for Medical Parasitology, Department of Infectious Diseases, University of Copenhagen, Copenhagen, Denmark

Natalie M. Barber, Clinton K. Y. Lau, and Louise Turner contributed equally to this work. Author order was determined alphabetically.

ABSTRACT Structure-guided vaccine design provides a route to elicit a focused immune response against the most functionally important regions of a pathogen surface. This can be achieved by identifying epitopes for neutralizing antibodies through structural methods and recapitulating these epitopes by grafting their core structural features onto smaller scaffolds. In this study, we conducted a modified version of this protocol. We focused on the PfEMP1 protein family found on the surfaces of erythrocytes infected with *Plasmodium falciparum*. A subset of PfEMP1 proteins bind to endothelial protein C receptor (EPCR), and their expression correlates with development of the symptoms of severe malaria. Structural studies revealed that PfEMP1 molecules present a helix-kinked-helix motif that forms the core of the EPCR-binding site. Using Rosetta-based design, we successfully grafted this motif onto a three-helical bundle scaffold. We show that this synthetic binder interacts with EPCR with nanomolar affinity and adopts the expected structure. We also assessed its ability to bind to antibodies found in immunized animals and in humans from malaria-endemic regions. Finally, we tested the capacity of the synthetic binder to effectively elicit antibodies that prevent EPCR binding and analyzed the degree of cross-reactivity of these antibodies across a diverse repertoire of EPCR-binding PfEMP1 proteins. Despite our synthetic binder adopting the correct structure, we find that it is not as effective as the CIDRα domain on which it is based for inducing adhesion-inhibitory antibodies. This cautions against the rational design of focused immunogens that contain the core features of a ligand-binding site of a protein family, rather than those of a neutralizing antibody epitope.

IMPORTANCE Vaccines train our immune systems to generate antibodies which recognize pathogens. Some of these antibodies are highly protective, preventing infection, while others are ineffective. Structure-guided rational approaches allow design of synthetic molecules which contain only the regions of a pathogen required to induce production of protective antibodies. On the surfaces of red blood cells infected by the malaria parasite *Plasmodium falciparum* are parasite molecules called PfEMP1 proteins. PfEMP1 proteins, which bind to human receptor EPCR, are linked to development of severe malaria. We have designed a synthetic protein on which we grafted the EPCR-binding surface of a PfEMP1 protein. We use this molecule to show which fraction of protective antibodies recognize the EPCR-binding surface and test its effectiveness as a vaccine immunogen.

KEYWORDS EPCR, PfEMP1, protein design

Parasites often expose proteins on their surfaces to mediate interactions with molecules of their mammalian host, allowing host cell invasion, nutrient uptake, and modulation of host immunity. The evolutionary driving forces which shape these parasite surface proteins are multiple, with the need to retain the capacity to interact with an unchanging mammalian binding partner balanced against the pressure to resist detection and clearance by the acquired immune system of the host. A common solution is the evolution of a family of proteins, which are deployed one at a time by the parasite through antigenic variation (1–3). This allows a population survival strategy in which parasites that express a protein recognized by host immunoglobulin are cleared, while those that express a functionally equivalent, but unrecognized, variant, survive. Such parasite surface protein families prove a major challenge to vaccine development, with their varying nature hampering efforts to design an immunogen that elicits a protective immune response across a family.

A classic example of a surface protein family is the PfEMP1 proteins of *Plasmodium falciparum* (1, 4). These are found on the surfaces of parasite-infected erythrocytes and interact with various human endothelial receptors. This causes infected erythrocytes to adhere to the surfaces of blood vessels and tissues, preventing their destruction by splenic clearance (5). Pathology in severe and placental malaria is associated with these adhesive properties, with endothelial binding occluding blood flow and inducing inflammatory responses (6). While there are many PfEMP1 proteins, and different family members bind to different human endothelial receptors (1, 4), a growing body of evidence suggests that severe and cerebral malaria are associated with expression of a subset of PfEMP1 that bind to the endothelial protein C receptor (EPCR) (7–15). Binding of PfEMP1 prevents EPCR from binding to its natural ligand, protein C (7, 8), thereby preventing PAR1-mediated endothelial signaling (16), most likely resulting in inflammation and endothelial dysfunction. Indeed, the EPCR-binding PfEMP1 are targeted by antibodies found in adults from malarial regions of endemicity (8), which are acquired early in life (8) and whose presence correlates with the individual having experienced a case of severe malaria (17). However, immunization of rodents with single CIDRα1 domains, free or attached to virus-like particles, does not generate antibody responses against the full repertoire of EPCR-binding domains (18, 19). This raises the question of whether it is possible to design vaccine immunogens that induce broadly inhibitory antibody responses that can target the sequence-diverse set of EPCR-binding PfEMP1 proteins.

The ectodomains of PfEMP1 proteins are formed from an array of two domain types, the DBL and CIDR domains (3), which have been grouped into a variety of subclasses (20). PfEMP1 are generally modular, with single domains containing the capacity to bind to individual receptors (8, 9, 21). The majority of CIDRα1 domain subclasses bind to EPCR (7, 8). Structural studies of these domains in complex with EPCR have revealed an interaction interface consisting of a hydrophobic core surrounded by a surface that mediates hydrogen bonds (8). At its center lies a helix-kinked-helix structural motif, which contains six of the eight EPCR-interacting residues. At the kink lies a phenylalanine residue, F656 in strain HB3var03, which is central to the binding site and whose mutation leads to a 100-fold increase in the dissociation-rate of the complex (8).

Analysis of the sequences of 885 CIDRα1 domains reveals that the interacting residues are not conserved, but nevertheless maintain conserved chemical characteristics, with retention of the hydrophobic nature of the protrusion and the surrounding hydrophilic surface (8). This raises the question of whether it is possible to design a protein which mimics this surface, and if such a protein can specifically elicit antibodies that block EPCR binding. Such antibodies would be functionally valuable in preventing the modulation of EPCR-mediated signaling implicated in the development of severe symptoms. In addition, antibodies that target the most conserved part of the CIDRα1 domain surface would have the greatest likelihood of being cross-reactive across the EPCR-binding PfEMP1 family.

A recent advance in structure-guided immunogen design is an approach in which

structures are determined for pathogen surface proteins in complex with antibodies with protective or broadly neutralizing properties, followed by the grafting of the epitopes of these antibodies onto smaller scaffolds (22, 23). In a number of cases, this has allowed the development of smaller immunogens which can specifically elicit the production of antibodies with desirable properties (24–27). The conserved chemistry and shape of the EPCR-binding site of the PfEMP1 (8) encouraged us to make a similar attempt. In this case, however, the absence of structural insight into the epitopes of inhibitory antibodies led us to trial a variant of this usual approach, in which we designed a smaller protein which mimics the features of the EPCR-binding site, while removing other potential epitopes found in CIDRα1 domains. In this we aimed to design a molecule which could be used as a tool to assess the role of antibodies that target the core of the EPCR-binding site. We also aimed to test this molecule as a vaccine immunogen to attempt to specifically elicit antibodies against the EPCR-binding site and assess their degree of cross-reactivity across the EPCR-binding PfEMP1 proteins.

RESULTS

Iterative design of a novel EPCR-binding protein. Our design strategy was informed by structural studies of complexes of CIDRα1 domains bound to EPCR (8). Eight amino acids from CIDRα1 domains directly contact EPCR, with six of these present in a motif consisting of a helix linked to a helix with a kink. We reasoned that we could graft this helix-kinked-helix motif onto a scaffold protein to generate an EPCR-binding protein containing the majority of the functional determinants of the CIDRα1 domain. To confirm that the two EPCR-contacting residues which would be missing from this design, D576A and K642A, were not essential for EPCR binding, we prepared mutated versions of the HB3var03 strain CIDRα1 domain in which they were replaced by alanine. The double mutant of these two residues showed a reduction in affinity, from 0.4 nM to 220 nM (Fig. S1 in the supplemental material). As this nanomolar affinity was in line with the range of affinities of CIDRα1 domains for EPCR measured previously (8), we continued with the design process.

To select a suitable scaffold on which we could recapitulate this helix-kinked-helix motif, we searched known protein folds, using PDBeFold and DALI (28). However, this identified no template with a matching surface-exposed structural motif. However, a three-helical bundle scaffold (PDB code 3LHP, chain S) used previously for immunogen grafting (29) contained α-helices whose path matched those of the two longer helices of the helix-kinked-helix motif, with the two helical portions overlaying with a root mean square deviation (RMSD) of 2.5 Å. We therefore grafted the helix-kinked-helix motif onto this scaffold and used a Rosetta-based strategy (25, 30) to redesign the resultant molecule to obtain the appropriate fold (Fig. 1A).

The starting model for the designed immunogen contained residues N648 to K678 from the HB3var03 CIDRα1.4 domain inserted in between residues Gly70 and Asp103 of the three-helical bundle (Fig. 1A, Fig. S2). This hybrid was assembled *in silico* and this starting model was allowed to reach a minimum energy conformation through being computationally refolded in Rosetta by allowing other features of the immunogen to fold around a rigidly held epitope region (residues N648 to K678 of HB3var03). This procedure was supplemented by Cα-Cα restraints derived from the original helical bundle to drive the model toward the target conformation. After generation of each model, restraints were removed, the epitope was unlocked, and the structure was allowed to relax to a local energy nadir. A plot of Rosetta score (a measure of the intramolecular interaction strength) against standard deviation to the starting model generated two clusters, one with root mean square deviation (RMSD) values of 0.5 to 2.5 Å to the starting model and one at significantly higher RMSD, with a helix displaced. The model with the lowest RMSD was chosen for subsequent design.

We next used the fold-from-loops procedure to adjust the initial design to improve its folding, while allowing residues not involved in the EPCR-binding site to vary in
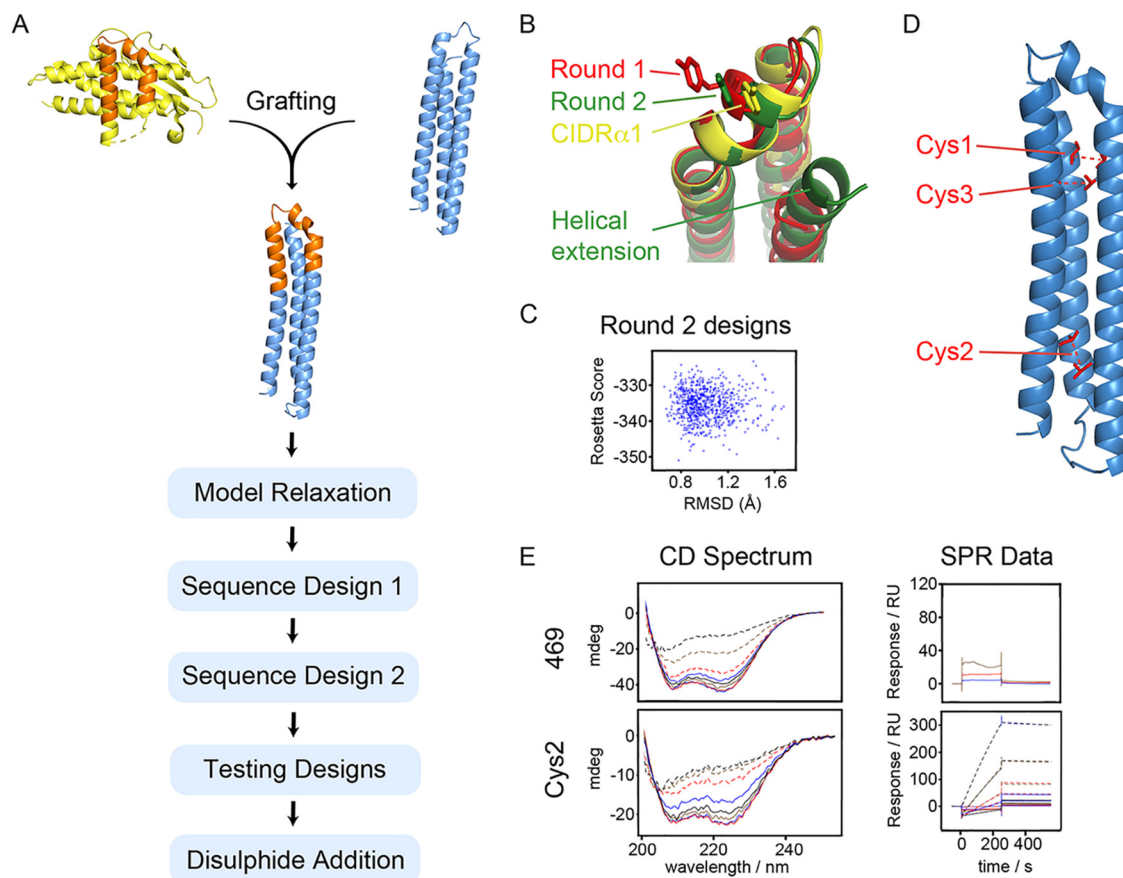
FIG 1 Design of a synthetic EPCR binder. (A) Schematic showing the design process. The EPCR-binding surface (orange) of the HB3var03 CIDRα1 domain (yellow) was grafted onto a three-helical bundle scaffold (blue), followed by a Rosetta-based design strategy. (B) Illustration of the outcome of design rounds 1 (red) and 2 (green) illustrating the importance of increasing the length of the C-terminal helix in generating a design that more closely mimics the CIDRα1 domain (yellow). (C) Analysis of output models from round 2, showing the Rosetta score and the root mean square deviation (RMSD) to the original epitope. (D) A model of the designed binder, indicating positions of residues mutated to cysteine to introduce stabilizing disulfide bonds. (E) Circular dichroism spectra and surface plasmon resonance analysis of EPCR-binding of the best design from round 2 (469) and the best disulfide-stabilized design (Cys2).

their identity (sequence design 1). Each residue was classed as a "surface," "boundary," or "interior" residue and was allowed to change to other amino acids within the same class. We prevented variation of eight residues that lie on the surface of the helix-kinked-helix in the CIDRα1 domain, six of which contact EPCR (corresponding to N648, D649, D652, S653, F655, F656, Q657, and Y660 from HB3var03 CIDRα1.4), and three residues likely to be important to maintain the conformation of the kinked helix (F651, V658, and W669 from HB3var03) (Fig. S2). Other residues, both surface-exposed and buried, which do not contribute to the EPCR-binding surface, were allowed to vary (Fig. S2). Four rounds of sequence design involved mutation followed by structural relaxation in Rosetta and determination of Rosetta score. Early rounds were constrained by Cα-Cα restraints derived from the desired conformation of the helix-kinked-helix, but these constraints were removed in the final stage, allowing the models to adopt a minimum energy conformation. These models were assessed based on their Rosetta score and their RMSD to the helix-kinked-helix motif. Assessment of the outputs from the first round of design shows deviations in the kinked helix from the original (Fig. 1B). This was resolved by increasing the length of the third helix of the helical bundle, which lies behind the helix-kinked-helix motif to provide additional support. Performing the same process of sequence design (sequence design 2) using this longer scaffold generated models which more closely match the starting design (Fig. 1B and C).

The design process generated a set of output models with as little as 35% pairwise sequence identity (Fig. S2). To select which models to test experimentally, we selected the 100 best based on RMSD to the epitope. These were classified by evolutionary trace analysis into eight groups, based simply on sequence, and a member of each of the eight groups was selected, which had a low RMSD to the epitope and a high pack-stat filter score (Fig. 1C), indicating a well-packed structure. These eight designs had pairwise sequence similarities of 35 to 60% (Fig. S2).

Genes corresponding to these eight designs were ordered, with codon optimization for expression in *Escherichia coli* and the inclusion of an N-terminal histidine tag (Table S1). Seven of these designs could be expressed in a soluble form and were purified. In each case, purification by size exclusion chromatography revealed a single monodispersed species. Circular dichroism spectroscopy revealed the seven designs to have a predominantly α-helical profile (Fig. S3). Thermal melts, analyzed by circular dichroism (CD), revealed the temperatures at which α-helicity was lost and showed major variation in stability across the seven designs, with, for example, 398 retaining more than 90% of helical character at 90°C and 469 melting at around 70°C. In contrast, others, such as 555, showed a broad, noncooperative transition toward loss of helicity, starting at 20°C (Fig. S3). Next, to assess if the designs had adopted the correct fold, we assessed their ability to bind to EPCR as measured by surface plasmon resonance. However, while the parent HB3var03 CIDRα1.4 domain binds to EPCR with an affinity of 0.36 nM, no binding was seen for any of the seven designs at 500 nM, suggesting that the EPCR-binding surface had not been correctly mimicked (Fig. S3).

We reasoned that the inability of any of the seven designs to bind to EPCR might suggest the designs did not adopt the desired structure. We therefore further stabilized the designs by the addition of disulfide bonds (Fig. 1D). We selected three sites in design 469 at which residues were predicted to be found at an appropriate distance to allow disulfide bond formation. These residues were replaced with cysteine to form three mutants, cys1, cys2, and cys3, each of which had a single disulfide bond. These were tested as above (Fig. S4). The cys2 variant was most effective, retaining α-helicity at up to 70°C in circular dichroism measurements and interacting with EPCR with a slow off-rate, reminiscent of the CIDRα1-EPCR interaction (Fig. 1E, Fig. 2A to C). As determined by surface plasmon resonance, the cys2 variant bound to EPCR with an affinity of 26 nM (Fig. 2A), which compares well with 220 nM for the D576A K642A mutant of this domain, which shares the same number of EPCR-binding residues as cys2 (Fig. S1). We therefore proceeded with this design for structural and functional testing.

Structure of the synthetic EPCR binder in complex with EPCR. We next determined the crystal structure of the synthetic binder in complex with EPCR (Fig. 2, Fig. S5, Table S2). We cleaved purified synthetic binder and EPCR with tobacco etch virus (TEV) protease to remove tags, and deglycosylated EPCR. These were combined, and the complex purified by size exclusion chromatography before being subjected to crystallization trials. Crystals formed and a complete data set was collected to 3.11 Å resolution. Molecular replacement, using the EPCR structure (8) as a search model, identified two copies of EPCR in the asymmetric unit of the crystal. Surprisingly, a cycle of refinement and model building revealed the presence of a single copy of the synthetic binder, with the asymmetric unit containing a complex of EPCR bound to a synthetic binder, together with a second, unliganded, copy of EPCR (Fig. S5).

The structure of the synthetic binder was compared with the model that emerged from the design process (Fig. 2D). A structural alignment revealed the EPCR-binding site to adopt an extremely similar conformation to that predicted, with the residues of the helix-kinked-helix motif of the synthetic binder (N72-W93) overlaying with the design with a RMSD of 1.19 Å. The structure also revealed that the synthetic binder bound to EPCR with the same binding mode as the HB3var03 CIDRα1 domain (Fig. 2E). Indeed, aligning these two complexes on the EPCR molecule showed the residues of the helix-kinked-helix of the synthetic binder (N72 to W93) to overlay with the corresponding residues of the HB3var03 CIDRα1.4 domain (N648-W669) with an RMSD of
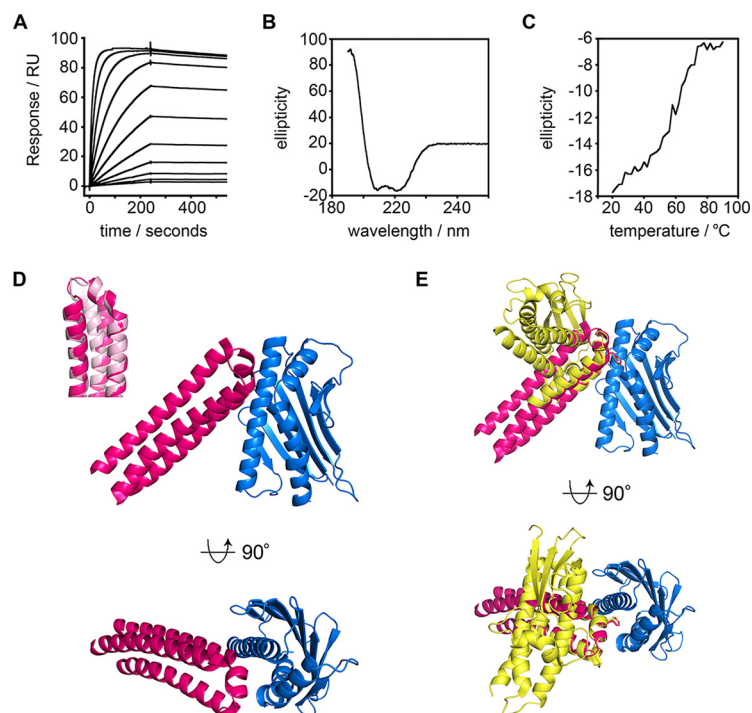
FIG 2 Structural and biophysical characterization of the synthetic binder. (A) Surface plasmon resonance analysis of the binding of the synthetic binder to EPCR. The data are for a 2-fold dilution series starting from 16 μM. (B) Circular dichroism analysis of the synthetic binder. (C) Thermal stability of the synthetic binder, determined by the circular dichroism signal at 222 nm wavelength at different temperatures. (D) Structure of EPCR (blue) bound to the synthetic binder (pink). The inset shows an overlay of the structure of the synthetic binder (pink) overlaid with the original design (light pink). (E) Overlay of the structures of EPCR (blue) in complexes bound the synthetic binder (pink) and the HB3var03 CIDRα1 domain (yellow), with EPCR molecules overlaid. The phenylalanine residues which enter into the hydrophobic groove of EPCR (F656 in HB3var03 and F80 in the synthetic binder) are shown as sticks.

0.77 Å. While in the absence of a structure of the synthetic binder in an unbound form we cannot rule out some adoption of structure on EPCR binding, the bound structure shows the designed synthetic binder to contain the core of the EPCR-binding site of the CIDRα1 domains and binds in the predicted manner to EPCR.

Assessment of antibody binding to the synthetic binder. We next asked whether our synthetic binder interacts with either antibodies present in rats immunized with CIDRα1 domains or with human antibodies from adult volunteers from malaria-endemic regions in Tanzania. This was to determine whether the helix-kinked-helix is the target of such antibodies and if these are inhibitory of EPCR binding.

Immunization of rats with the HB3var03 CIDRα1.4 domain induces the production of antibodies that prevent the cognate CIDRα1.4 domain from binding to EPCR (18) (Fig. 3A). We affinity-purified antibodies from this serum on columns coupled with either HB3var03 CIDRα1.4 or our synthetic binder. Affinity purification on the CIDRα1 domain resulted in a flowthrough that contained only ~20% of the inhibitory activity found in the original serum, suggesting that the majority of inhibitory antibodies were depleted by binding to CIDRα1 domain. In contrast, passage through a column containing the synthetic binder did not reduce the capacity of the flowthrough to inhibit EPCR binding by the CIDRα1 domain, suggesting that the majority of inhibitory antibodies in this serum do not bind to the synthetic binder. Nevertheless, the antibodies eluted from the synthetic binder did show some inhibitory capacity, causing 40% inhibition of the CIDRα1 domain binding to EPCR at a 50% dilution (Fig. 3A). This could be compared with nearly complete inhibition of EPCR binding at a 3.1% dilution of
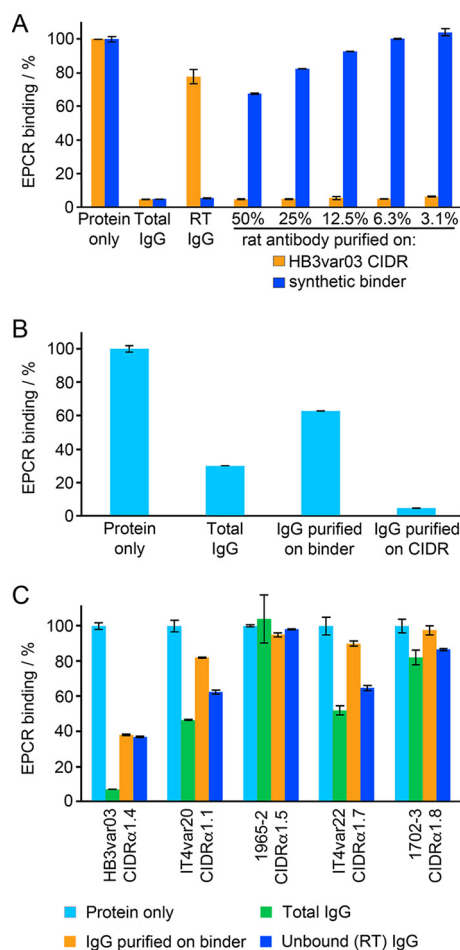
FIG 3 Targeting of the synthetic binder by antibodies from immunized rats or from humans from malarial regions of endemicity. (A) Antibodies from rats immunized with the HB3var03 CIDRα1.4 domain were affinity purified using either HB3var03 CIDRα1.4 domain or the synthetic binder. These were assessed for their ability to prevent the CIDRα1.4 domain from binding to EPCR. Protein alone indicates binding of EPCR in the absence of antibody. Total IgG shows EPCR binding in the presence of 0.55 mg/ml total IgG. RT IgG shows EPCR binding in the presence of antibodies that did not bind to the affinity column. The remaining columns show EPCR binding in the presence of affinity-purified antibodies at different dilutions. All data are expressed as a percentage of the binding in the absence of antibody. (B) Prevention of CIDRα1 binding to EPCR by purified rat antibodies was quantified at 25 μg/ml. Binding in the presence of total IgG or of IgG affinity purified on the synthetic binder or the HB3var03 CIDRα1.4 domain is expressed as a fraction of the binding in the absence of antibody (protein alone). (C) Sera taken from 15 individuals from malarial regions of endemicity in Tanzania were pooled and tested for their ability to prevent five different CIDRα1 domains from binding to EPCR. The total antibody pool was tested, as were antibodies purified on a column coupled with the synthetic protein and antibodies that did not bind to this column (RT IgG). In each case, this is expressed as a percentage of the binding in the absence of any antibody (protein alone).

antibodies purified on the CIDRα1 domain. Therefore, despite the synthetic binder adopting the correct confirmation, it was not recognized by the majority of CIDRα1-reactive antibodies that block EPCR binding in these sera.

We next quantified this effect by assessing the inhibitory capacity of the affinity-purified antibodies at fixed concentrations of 25 μg/ml (Fig. 3B). Total purified IgG caused an ~70% reduction in EPCR binding by the CIDRα1 domain. Antibodies purified by affinity for the CIDRα1 domain elicited a more than 90% reduction in EPCR binding at this concentration, while those purified by affinity for the synthetic binder caused an approximately 40% reduction. This suggests that sera raised through immunization of rats with the CIDRα1 domain contain antibodies that do not recognize the

helix-kinked-helix motif, and that these antibodies contribute significantly to the prevention of EPCR binding.

We next conducted a similar experiment in which we purified human antibodies from a pool of polyclonal sera taken from 15 semi-immune volunteers from a malaria-endemic region in Tanzania, with sera selected based on their inhibitory effect on EPCR binding by the HB3var03 CIDRα1.4 domain (Fig. 3C). This antibody pool was tested for the ability to prevent EPCR binding by five different CIDRα1 domains, taken from five different domain subclasses. These antibodies, acquired in response to natural infection, had various abilities to prevent CIDRα1 domains from binding to EPCR. The binding of HB3var03 (CIDRα1.4) to EPCR was reduced by >90%, while the binding of IT4var20 (CIDRα1.1) and IT4var22 (CIDRα1.7) were reduced by ~50%. A smaller inhibitory effect was seen for 1702_3 (CIDRα1.8), while there was no inhibitory effect on 1965_2 (CIDRα1.5).

We next affinity-purified antibodies from this human serum pool using a column coupled with the synthetic binder, and assessed the capacity of these antibodies to prevent CIDRα1 domains from binding to EPCR. In the case of the IT4var20 CIDRα1.1 domain, the affinity-purified antibodies retained about 40% of the inhibitory capacity of the original antibody mixture. In other cases, the majority of inhibitory antibodies were found in the run-through of the column. These findings suggest that in both CIDRα1 domain-immunized rats and in humans who have acquired antibodies as a result of natural exposure to parasites, the majority of antibodies that inhibit EPCR binding do not bind solely to the EPCR-binding region of the kinked helix. Nevertheless, antibodies which do bind to this region, found in the context of the synthetic binder, do block EPCR binding.

Synthetic binder induces inhibitory, but not cross-reactive, antibodies in immunized rats. As our synthetic binder was recognized by inhibitory antibodies from sera, we next assessed whether it would be effective as an immunogen to raise such antibodies. We immunized rats with the synthetic binder and assessed if the purified total antibodies from these sera blocked EPCR binding by the HB3var03 CIDRα1.4 domain. Antibodies purified from rats immunized with synthetic binder caused an ~40% decrease in EPCR binding by this CIDRα1 domain (Fig. 4A). We again purified antibodies from this serum, either using a column coupled with the synthetic binder or one coupled with the CIDRα1 domain. In this case, both columns depleted the majority of inhibitory antibodies from the serum, suggesting the inhibitory antibodies present do target the helix-kinked-helix motif (Fig. 4A).

We next assessed, at an equivalent concentration of 25 μg/ml, the effectiveness of these affinity-purified antibodies compared with those induced by immunization of a rat with the CIDRα1 domain, and affinity purified on either CIDRα1 domain or synthetic binder (Fig. 4B). This showed that, while immunization with the synthetic binder did generate antibodies which could inhibit CIDRα1 domains from binding to EPCR, these antibodies were less effective, both in pure serum and at equal concentration, than those generated through immunization with CIDRα1 domains. We had planned to next perform a series of prime-boost regimens, for example using a CIDRα1 domain prime and a synthetic protein boost, and vice versa, to attempt to generate more focused responses. However, the lower quality of antibodies generated through synthetic protein immunization suggested this was not the correct strategy. Instead, our findings supported the view that antibodies which target sites other than the helix-kinked-helix motif are inhibitory or potentiate the effect of such inhibitory antibodies.

Finally, we assessed the breadth of reactivity of the antibodies generated through immunization with the synthetic binder. One of the goals of designing an immunogen containing the helix-kinked-helix motif was to attempt to raise more broadly reactive antibody mixtures, as this region of the domain is most conserved in chemistry and structure (8). We therefore tested the ability of the serum raised through immunization with the synthetic binder to recognize a panel of CIDRα1 domains from different subclasses in a Luminex assay (Fig. 4C, Fig. S6). In this case, we found that as well as recognizing the cognate HB3var03 CIDRα1.4 domain, the sera recognized four other CIDRα1.4
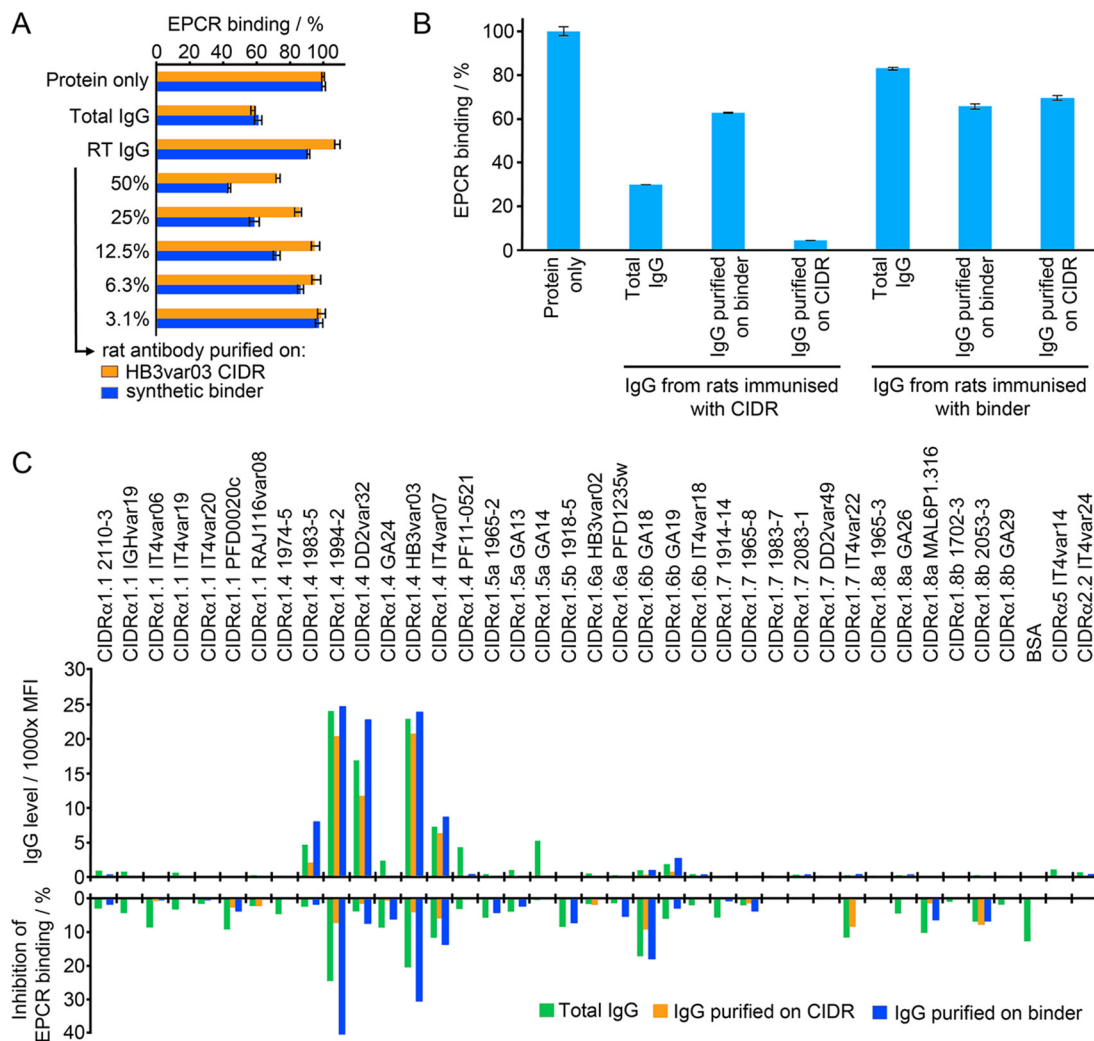
FIG 4 Immunogenicity of the synthetic binder. (A) Antibodies from rats immunized with synthetic binder were affinity purified using either the HB3var03 CIDRα1.4 domain or the synthetic binder. These were assessed for their ability to prevent the CIDRα1.4 domain from binding to EPCR. Protein alone indicates binding of EPCR in the absence of antibody. Total IgG shows EPCR binding in the presence of 0.40 mg/ml total IgG. RT IgG shows EPCR binding in the presence of antibodies that did not bind to the affinity column. The remaining columns show EPCR binding in the presence of affinity-purified antibodies at different dilutions. All data are expressed as a percentage of the binding in the absence of antibody (protein only). (B) Prevention of CIDRα1 binding to EPCR by rat antibodies was quantified at 25 μg/ml. Antibodies were from rats immunized either with the synthetic binder or the HB3var03 CIDRα1.4 domain. Binding in the presence of total IgG or of IgG affinity purified on the synthetic binder or the HB3var03 CIDRα1.4 domain is expressed as a fraction of the binding in the absence of antibody (protein alone). (C) IgG from rats immunized with synthetic binder was tested against a panel of CIDRα domains, either as total IgG or after affinity purification on the synthetic binder or a HB3var03 CIDRα1.4 domain. The CIDRα2 and α5 domains are not expected to bind EPCR. The upper panel shows IgG binding levels (in mean fluorescence intensity, MFI). The lower panel shows the inhibition of the binding of these CIDRα domains to EPCR.

domains. This cross-reactivity was retained in antibodies purified on either the synthetic binder or the HB3var03 CIDRα1 domain (Fig. 4C). However, there was no reactivity to the other 31 CIDRα1 domains in the panel, or to the two CD36-binding CIDR domains. In parallel, we conducted a similar experiment in which we expressed the synthetic binder with a spy-tag at the C terminus and coupled it to a spy-catcher-conjugated virus-like particle before immunization and testing. However, this revealed no increase in breadth of reactivity (Fig. S6). Therefore, antibodies induced through immunization with the synthetic binder were not more cross-reactive than those generated through immunization with CIDRα1 domains (18).

DISCUSSION

A recent approach in vaccine design is to use structural methods to understand how critical protective monoclonal antibodies bind to a vaccine target and to then design a synthetic protein which recapitulates the structural features of the antibody epitope (22, 23). This has been used in the past to design novel vaccine components and to specifically elicit broadly inhibitory antibodies through immunization (24–27). In this study, we attempted a variant of this approach. In the absence of inhibitory antibodies against EPCR-binding PfEMP1 proteins, we instead used our knowledge of the structural features of the EPCR-binding site (8) and grafted the core of this surface onto a three-helical bundle, which was redesigned through a Rosetta-based approach to produce a small synthetic protein that mimics the key features of the EPCR-binding surface. As the mimicked motif is the most conserved and functionally important surface feature of this protein family, we reasoned that antibodies that bind this region have the potential to be inhibitory and cross-reactive against the large and sequence-diverse spectrum of EPCR-binding PfEMP1 proteins.

The design and production of the synthetic protein was successful. Surface plasmon resonance measurements showed that it bound to EPCR with a high nanomolar affinity that matched prediction. In addition, a crystal structure of the synthetic protein in complex with EPCR showed that it adopted a structure close to that expected, and bound in a mode that matched that of the parent CIDRα1 domain. We have therefore generated a synthetic protein which contains the core structural features of an EPCR-binding PfEMP1 domain.

We next tested the ability of this synthetic binder to interact with antibodies from sera of animals immunized with CIDRα1 domains, or from human volunteers from a malarial region of endemicity in Tanzania. We found that both serum types contained antibodies that bound to the synthetic protein, and that a fraction of these antibodies were inhibitory of EPCR binding. However, these antibodies were less effective than those purified through binding to the CIDRα1 domain, both in quantity and quality.

Further, we immunized rats with either the HB3var03 CIDRα1 domain or the synthetic binder and assessed the capacity of antibodies to recognize multiple CIDRα1 domains and to block their binding to EPCR. Immunization of rats with the synthetic binder did generate antibodies that bind to their cognate CIDRα1 domain and prevent it from binding to EPCR. However, these were less effective and less abundant than equivalent antibodies raised through immunization with a CIDRα1 domain. In addition, when tested against a panel of CIDRα1 domains, the antibodies raised through immunization with the synthetic binder showed no more cross-reactivity than those raised through immunization with a CIDRα1 domain. Therefore, there is no evidence to suggest that focusing the immune response onto the kinked-helix motif generates more cross-reactive and cross-inhibitory antibodies in rodents.

These findings suggest that many of the epitopes for inhibitory antibodies on the EPCR-binding CIDRα1 domains are not solely located on the EPCR-binding region of the helix-kinked-helix motif. There are a number of possible explanations for this finding. First, the residues from the CIDRα domain which contact EPCR were retained in the synthetic binder, but other surface residues from the CIDRα domain were not retained, and may be important to form an epitope mimic. In addition, the angle at which the binding site is presented to EPCR or to antibodies differs between the synthetic binder and the CIDRα domain. Finally, it is possible that this region of the protein does not closely complement any germ line antibodies in the mouse genome. This study therefore cautions against an approach in which a binding surface is grafted onto a smaller scaffold for immunization. In contrast, knowledge of the structure of the epitope of an effective antibody known to be elicited through human immunization is a valid starting point for such a study, allowing certainty that a complete epitope is recapitulated and also that it is possible to elicit such an antibody from the human germ line. The quest to generate an epitope-focused vaccine targeting an EPCR-binding PfEMP1 protein therefore requires isolation and detailed molecular characterization

of human monoclonal antibodies that target these domains as a starting point for future structure-guided vaccine development efforts.

MATERIALS AND METHODS

Rosetta-based design. Epitope grafting used the Rosetta package (31) and was based on the fold-from-loops protocol (25). A composite model was generated in which the helix-kinked-helix motif was manually inserted into the three-helical bundle of PDB code 3LHP, chain S using Coot (29). An initial model was created by folding the helical bundle sequence around the fixed epitope using $C\alpha$-$C\alpha$ restraints derived from the initial model. The resultant models were scored based on their Rosetta score and their root mean square deviation (RMSD) from the starting model. Sequence design was performed using a script from RosettaScripts (32), allowing all residues to change except for 72, 73, 75, 76, 77, 79, 80, 81, 82, 84, and 93. Four rounds of sequence design were conducted, using $C\alpha$-$C\alpha$ restraints derived from the initial model. Ten thousand output models were generated and were filtered using Rosetta scores. Those with scores lower than the starting model were then filtered using the packstat filter (33). As a final step, the best-packed models were relaxed in the absence of $C\alpha$-$C\alpha$ restraints and were filtered again using the packstat filter.

Protein production. The HB3var03 CIDRα1.4 domain and its mutants were expressed in the BL21 strain of *E. coli* (8). The gene for the CIDRα domain was available in a modified pEt15b vector with an N-terminal hexa-histidine tag and a tobacco etch virus (TEV) cleavage site. Mutagenesis was performed using the Quikchange method to produce the D576A and K642A single and double mutants. Transformed *E. coli* were grown to an optical density of 1.0 at 600 nm wavelength (OD$_{600}$) and expression was induced at 27°C by addition of IPTG (isopropyl-β-D-thiogalactopyranoside) to a final concentration of 1 mM. Cells were harvested 3 h after induction. The CIDRα1 domains were expressed in the form of inclusion bodies, which were unfolded by incubation at room temperature in 6 M guanidine-hydrochloride, 20 mM Tris (pH 8), 300 mM NaCl, and 15 mM imidazole for 15 h. Refolding was achieved by gradual buffer exchange into 20 mM Tris (pH 8), 300 mM NaCl, and 15 mM imidazole in the presence of a glutathione redox buffer (3 mM reduced glutathione, 0.3 mM oxidized glutathione) while the protein was bound to a Ni-NTA column. Refolded protein was eluted and further purified by size exclusion gel chromatography (HiLoad Superdex 75 16/60, GE Healthcare) into 20 mM HEPES (pH 7.5), 150 mM NaCl.

CIDRα1 domains used for immunization and EPCR-binding assays were produced in baculovirus-infected High Five cells as His$_6$-tagged 30 kDa proteins (8) or 19 kDa STREP-II-tagged proteins lacking the N-terminal β-sheet (18).

Designed synthetic binders were produced in *E. coli*. Synthetic genes were codon optimized for *E. coli* (GeneArt) and were inserted into the pEt15b vector to give an N-terminal His$_6$ tag and a TEV cleavage site. Cysteine mutations to introduce disulfide bonds were incorporated using Quikchange mutagenesis (I10C L74C for Cys1; L53C L115C for Cys2; and V71C A100C for Cys3). The final synthetic binder was also cloned with a C-terminal spy-tag to allow attachment to virus-like particles decorated with spy-catcher (34, 35). The designed proteins were all expressed in inclusion bodies by growth at 25°C overnight after induction with 1 mM IPTG. Protein was purified using the same on-column refolding method as for the CIDRα1 domains.

EPCR was expressed from a stable *Drosophila* s2 cell line, generating residues 16 to 210 fused to an N-terminal BAP tag, a His$_6$ tag, and a TEV cleavage site (8). Culture medium was buffer exchanged into 20 mM Tris (pH 8)/500 mM NaCl and protein was purified by Ni-NTA affinity chromatography and size exclusion gel chromatography (HiLoad Superdex 75 16/60, GE Healthcare) using 20 mM HEPES (pH 7.5)/150 mM NaCl. Protein for crystallography was deglycosylated by treatment with endoglycosidase H$_f$ (Sigma) and endoglycosidase F3 at enzyme:protein ratios of 1:50 in 50 mM MES (morpholineethanesulfonic acid; pH 6.5) for 15 h. N-terminal tags were cleaved using TEV protease at an enzyme:protein ratio of 1:50 in phosphate-buffered saline (PBS) (Melford) with 3 mM reduced glutathione/0.3 mM oxidized glutathione for 15 h at 25°C.

Surface plasmon resonance analysis. EPCR was biotinylated on the BAP tag by incubating 1 mg EPCR (30 μM) in 20 mM HEPES (pH 7.5)/150 mM NaCl with 20 μg BirA, 0.3 μM biotin, and 5 mM ATP for 15 h at 25°C and was then coupled to CAPture chip (GE Healthcare). This strategy was designed to allow EPCR to be immobilized with an orientation matching that found on the endothelial surface, and to generate a surface that could readily be regenerated.

Surface plasmon resonance (SPR) experiments were carried out on a Biacore T200 instrument (GE Healthcare). All experiments were performed in 20 mM HEPES (pH 7.5), 150 mM NaCl, 0.005% Tween 20 at 25°C. Twofold dilution series of each CIDRα domain or synthetic binder were prepared for injection over an EPCR-coated chip. For each cycle, biotinylated recombinant EPCR was immobilized on a CAP chip using the Biotin Capture kit (GE Healthcare) to a total loading of 150 RU. Binding partners were injected for 240 s with a dissociation time of 300 s. The chip was regenerated in between cycles using regeneration solution from the Biotin Capture kit (GE Healthcare). The specific binding response of the synthetic binders to EPCR was determined by subtracting the response given by the binder from a surface to which no EPCR had been coupled. The kinetic sensorgrams were globally fitted to a 1:1 interaction model to allow calculation of the association rate constant, k_a; the dissociation rate constant, k_d; and the dissociation constant K_D using BIAevaluation software version 1.0 (GE Healthcare).

Circular dichroism analysis. Circular dichroism measurements were taken using a J-815 spectrophotometer (JASCO) with attached Peltier water bath. Proteins were buffer exchanged into 10 mM phosphate (pH 7.5)/150 mM NaF and were held in a quartz cuvette. Buffer-subtracted spectra were collected at wavelengths from 190 nm to 260 nm, at 25°C with 10 spectra averaged for each measurement. For thermal melt experiments, spectra were taken at 2°C intervals from 20°C to 90°C.

Crystallization and structure determination. For crystallization, TEV-cleaved synthetic binder was mixed with EPCR that had been TEV cleaved and deglycosylated at a molar ratio of 1.1 to 1, synthetic binder to EPCR. The complex was separated by size exclusion chromatography using a Superdex 200 16/60 column (GE Healthcare) into a buffer containing 20 mM HEPES/150 mM NaCl (pH 7.5) and was concentrated to 10.7 mg/ml. Crystals grew in sitting drops with a well solution of 2 M sodium citrate/0.1 M HEPES (pH 7) at 4°C. Crystals were cryo-protected by transfer into 2 M sodium citrate, 0.1 M HEPES (pH 7), and 25% glycerol and were cryo-cooled in liquid nitrogen.

A complete data set was collected to 3.11 Å resolution and data were indexed and scaled using Xia2 (36). Molecular replacement was performed in Phaser (37) using the structure of EPCR (PDB: 4V3D) (8) as a search model, identifying two copies in the asymmetric unit. Refinement in BUSTER (38), using the missing atoms functionality, revealed electron density corresponding to a single copy of the synthetic binder in complex with one of the copies of EPCR. A cycle of model building and refinement in COOT (39) and BUSTER allowed completion of the model of the synthetic binder, except for residues 35 to 50, which remained disordered.

Coupling to virus-like particles and immunization of rats. Synthetic binder was coupled to *Acinetobacter* bacteriophage AP205 virus-like particles (VLPs) displaying one N-terminal SpyCatcher per capsid subunit (35). VLPs were expressed in *E. coli* BL21 StarTM (DE3) cells (Thermo Fisher Scientific) and purified by ultracentrifugation using an OptiprepTM density gradient (Sigma). Assembled VLPs and synthetic binder antigen were mixed at a 1:1 molar ratio and incubated for 2 h at room temperature.

Assembled VLPs were quality assessed by dynamic light scattering (DLS). The vaccine was centrifuged at 15,000 × *g* for 10 min and the supernatant was loaded into a disposable Eppendorf Uvette cuvette (Sigma-Aldrich, USA) and measured 20 times at 25°C using a DynoPro NanoStar (WYATT Technology, USA) with a 658 nm wavelength laser. Intensity-average size (nm) and percentage polydispersity (%Pd) were estimated using Dynamic software (Version 7.5.0).

Groups of four rats were immunized with 19-kDa HB3var03 CIDRα1.4 STRPII-tagged protein (18), with synthetic binder coupled to VLPs or with synthetic binder alone. In all groups, rats received 20 μg protein in each immunization. The rats were immunized intramuscularly (i.m.) every third week in a prime boost setting with Freund's incomplete adjuvant for a total of three immunizations.

Immunoglobulin purification. One milliliter of serum was taken from each rat. From each immunization group of four rats, these were pooled and the IgG was purified using protein G Sepharose and was eluted into PBS to a total volume of 4 ml. Purified total IgG (1,750 μl) was passed over *N*-hydroxysuccinimide-activated agarose columns loaded with 0.5 mg of either His$_6$-tagged 30 kDa HB3var03 CIDRα1.4 or synthetic binder protein. Bound IgG was eluted and concentrated to 500 μl in PBS, and the inhibitory effects of these preparations were tested at different dilutions (Fig. 3A, 4A, and 4C). Alternatively, these purified IgG were further concentrated using Vivaspin columns before testing at equal protein concentrations (Fig. 3B and 4B). Human IgG was similarly purified from plasma obtained from 15 malaria-exposed Tanzanian donors selected by the ability of the plasma to inhibit HB3var03 CIDRα1.4 from binding to EPCR by enzyme-linked immunosorbent assay (ELISA).

Assessment of CIDRα domain reactivity and of the inhibition of EPCR-binding by CIDRα1 domains. An ELISA-based assay was used to assess the inhibition of the binding of His$_6$-tagged 30 kDa recombinant HB3var03 CIDRα1.4 (8) to EPCR. ELISA plates were coated with 3 μg/ml recombinant EPCR, incubated overnight at 4°C, and were blocked with phosphate-buffered saline (PBS) containing 3% skimmed milk. CIDRα1 protein was added at 5 μg/ml concentration, with or without the addition of antibodies, and was incubated for 1 h before washing three times with PBS containing 0.05% Tween 20. EPCR binding was determined using horseradish peroxidase (HRP)-conjugated anti-His$_6$ antibody (1:3,000). All ELISAs were conducted to reach optical densities between 0.9 and 1.3 for the positive control without antibody addition and data are presented with this control normalized to 100%.

To assess cross-reactivity, IgG binding to a panel of 38 CIDRα domains coupled to Luminex microspheres was measured (40). Serum was diluted 1:20 and IgG reactivity was detected using secondary phycoerythrin (PE)-conjugated antibody diluted to 1:3,000. To assess inhibition of EPCR binding, microspheres were incubated with IgG at 1:50 for 30 min at room temperature. After washing with standard Luminex buffers, microspheres were incubated with 4 μg/ml biotinylated recombinant EPCR for 30 min at room temperature. EPCR binding was detected using PE-conjugated streptavidin.

Data availability. Data for the structure reported here has been deposited in the PDB under the accession code 6SNY. Additional data supporting the findings reported in the manuscript are available from the corresponding author on request.

SUPPLEMENTAL MATERIAL

Supplemental material is available online only.

FIG S1, TIF file, 2 MB.
FIG S2, TIF file, 2.9 MB.
FIG S3, TIF file, 2.4 MB.
FIG S4, TIF file, 2.8 MB.
FIG S5, TIF file, 2.9 MB.
FIG S6, TIF file, 2.6 MB.
TABLE S1, DOCX file, 0.1 MB.
TABLE S2, DOCX file, 0.1 MB.

REFERENCES

1. Wahlgren M, Goel S, Akhouri RR. 2017. Variant surface antigens of Plasmodium falciparum and their roles in severe malaria. Nat Rev Microbiol 15:479–491. https://doi.org/10.1038/nrmicro.2017.47.
2. McCulloch R, Cobbold CA, Figueiredo L, Jackson A, Morrison LJ, Mugnier MR, Papavasiliou N, Schnaufer A, Matthews K. 2017. Emerging challenges in understanding trypanosome antigenic variation. Emerg Top Life Sci 1:585–592. https://doi.org/10.1042/ETLS20170104.
3. Higgins MK, Carrington M. 2014. Sequence variation and structural conservation allows development of novel function and immune evasion in parasite surface protein families. Protein Sci 23:354–365. https://doi.org/10.1002/pro.2428.
4. Smith JD, Rowe JA, Higgins MK, Lavstsen T. 2013. Malaria's deadly grip: cytoadhesion of Plasmodium falciparum-infected erythrocytes. Cell Microbiol 15:1976–1983. https://doi.org/10.1111/cmi.12183.
5. Saul A. 1999. The role of variant surface antigens on malaria-infected red blood cells. Parasitol Today 15:455–457. https://doi.org/10.1016/s0169-4758(99)01534-3.
6. Miller LH, Baruch DI, Marsh K, Doumbo OK. 2002. The pathogenic basis of malaria. Nature 415:673–679. https://doi.org/10.1038/415673a.
7. Turner L, Lavstsen T, Berger SS, Wang CW, Petersen JE, Avril M, Brazier AJ, Freeth J, Jespersen JS, Nielsen MA, Magistrado P, Lusingu J, Smith JD, Higgins MK, Theander TG. 2013. Severe malaria is associated with parasite binding to endothelial protein C receptor. Nature 498:502–505. https://doi.org/10.1038/nature12216.
8. Lau CK, Turner L, Jespersen JS, Lowe ED, Petersen B, Wang CW, Petersen JE, Lusingu J, Theander TG, Lavstsen T, Higgins MK. 2015. Structural conservation despite huge sequence diversity allows EPCR binding by the PfEMP1 family implicated in severe childhood malaria. Cell Host Microbe 17:118–129. https://doi.org/10.1016/j.chom.2014.11.007.
9. Lennartz F, Adams Y, Bengtsson A, Olsen RW, Turner L, Ndam NT, Ecklu-Mensah G, Moussiliou A, Ofori MF, Gamain B, Lusingu JP, Petersen JE, Wang CW, Nunes-Silva S, Jespersen JS, Lau CK, Theander TG, Lavstsen T, Hviid L, Higgins MK, Jensen AT. 2017. Structure-guided identification of a family of dual receptor-binding PfEMP1 that is associated with cerebral malaria. Cell Host Microbe 21:403–414. https://doi.org/10.1016/j.chom.2017.02.009.
10. Jespersen JS, Wang CW, Mkumbaye SI, Minja DT, Petersen B, Turner L, Petersen JE, Lusingu JP, Theander TG, Lavstsen T. 2016. Plasmodium falciparum var genes expressed in children with severe malaria encode CIDRalpha1 domains. EMBO Mol Med 8:839–850. https://doi.org/10.15252/emmm.201606188.
11. Bernabeu M, Danziger SA, Avril M, Vaz M, Babar PH, Brazier AJ, Herricks T, Maki JN, Pereira L, Mascarenhas A, Gomes E, Chery L, Aitchison JD, Rathod PK, Smith JD. 2016. Severe adult malaria is associated with specific PfEMP1 adhesion types and high parasite biomass. Proc Natl Acad Sci U S A 113:E3270–E3279. https://doi.org/10.1073/pnas.1524294113.
12. Kessler A, Dankwa S, Bernabeu M, Harawa V, Danziger SA, Duffy F, Kampondeni SD, Potchen MJ, Dambrauskas N, Vigdorovich V, Oliver BG, Hochman SE, Mowrey WB, MacCormick IJC, Mandala WL, Rogerson SJ, Sather DN, Aitchison JD, Taylor TE, Seydel KB, Smith JD, Kim K. 2017. Linking EPCR-binding PfEMP1 to brain swelling in pediatric cerebral malaria.

Cell Host Microbe 22:601–614. https://doi.org/10.1016/j.chom.2017.09.009.
13. Tuikue Ndam N, Moussiliou A, Lavstsen T, Kamaliddin C, Jensen ATR, Mama A, Tahar R, Wang CW, Jespersen JS, Alao JM, Gamain B, Theander TG, Deloron P. 2017. Parasites causing cerebral Falciparum malaria bind multiple endothelial receptors and express EPCR and ICAM-1-binding PfEMP1. J Infect Dis 215:1918–1925. https://doi.org/10.1093/infdis/jix230.
14. Shabani E, Hanisch B, Opoka RO, Lavstsen T, John CC. 2017. Plasmodium falciparum EPCR-binding PfEMP1 expression increases with malaria disease severity and is elevated in retinopathy negative cerebral malaria. BMC Med 15:183. https://doi.org/10.1186/s12916-017-0945-y.
15. Mkumbaye SI, Wang CW, Lyimo E, Jespersen JS, Manjurano A, Mosha J, Kavishe RA, Mwakalinga SB, Minja DT, Lusingu JP, Theander TG, Lavstsen T. 2017. The severity of Plasmodium falciparum infection is associated with transcript levels of var genes encoding endothelial protein C receptor-binding P falciparum erythrocyte membrane protein 1. Infect Immun 85:e00841-16. https://doi.org/10.1128/IAI.00841-16.
16. Petersen JE, Bouwens EA, Tamayo I, Turner L, Wang CW, Stins M, Theander TG, Hermida J, Mosnier LO, Lavstsen T. 2015. Protein C system defects inflicted by the malaria parasite protein PfEMP1 can be overcome by a soluble EPCR variant. Thromb Haemost 114:1038–1048. https://doi.org/10.1160/TH15-01-0018.
17. Rambhatla JS, Turner L, Manning L, Laman M, Davis TME, Beeson JG, Mueller I, Warrel J, Theander TG, Lavstsen T, Rogerson SJ. 2019. Acquisition of antibodies against endothelial protein C receptor-binding domains of Plasmodium falciparum erythrocyte membrane protein 1 in children with severe malaria. J Infect Dis 219:808–818. https://doi.org/10.1093/infdis/jiy564.
18. Turner L, Theander TG, Lavstsen T. 2018. Immunization with recombinant Plasmodium falciparum erythrocyte membrane protein 1 CIDRalpha1 domains induces domain subtype inhibitory antibodies. Infect Immun 86:e00435-18. https://doi.org/10.1128/IAI.00435-18.
19. Harmsen C, Turner L, Thrane S, Sander AF, Theander TG, Lavstsen T. 2020. Immunization with virus-like particles conjugated to CIDRalpha1 domain of Plasmodium falciparum erythrocyte membrane protein 1 induces inhibitory antibodies. Malar J 19:132. https://doi.org/10.1186/s12936-020-03201-z.
20. Rask TS, Hansen DA, Theander TG, Gorm Pedersen A, Lavstsen T. 2010. Plasmodium falciparum erythrocyte membrane protein 1 diversity in seven genomes–divide and conquer. PLoS Comput Biol 6:e1000933. https://doi.org/10.1371/journal.pcbi.1000933.
21. Hsieh FL, Turner L, Bolla JR, Robinson CV, Lavstsen T, Higgins MK. 2016. The structural basis for CD36 binding by the malaria parasite. Nat Commun 7:12837. https://doi.org/10.1038/ncomms12837.
22. Burton DR. 2017. What are the most powerful immunogen design vaccine strategies? Reverse vaccinology 2.0 shows great promise. Cold Spring Harb Perspect Biol 9:a030262. https://doi.org/10.1101/cshperspect.a030262.
23. Sesterhenn F, Bonet J, Correia BE. 2018. Structure-based immunogen design—leading the way to the new age of precision vaccines. Curr Opin Struct Biol 51:163–169. https://doi.org/10.1016/j.sbi.2018.06.002.
24. Correia BE, Ban YE, Holmes MA, Xu H, Ellingson K, Kraft Z, Carrico C, Boni E, Sather DN, Zenobia C, Burke KY, Bradley-Hewitt T, Bruhn-Johannsen JF,

Kalyuzhniy O, Baker D, Strong RK, Stamatatos L, Schief WR. 2010. Computational design of epitope-scaffolds allows induction of antibodies specific for a poorly immunogenic HIV vaccine epitope. Structure 18:1116–1126. https://doi.org/10.1016/j.str.2010.06.010.

25. Correia BE, Bates JT, Loomis RJ, Baneyx G, Carrico C, Jardine JG, Rupert P, Correnti C, Kalyuzhniy O, Vittal V, Connell MJ, Stevens E, Schroeter A, Chen M, Macpherson S, Serra AM, Adachi Y, Holmes MA, Li Y, Klevit RE, Graham BS, Wyatt RT, Baker D, Strong RK, Crowe JE, Jr, Johnson PR, Schief WR. 2014. Proof of principle for epitope-focused vaccine design. Nature 507:201–206. https://doi.org/10.1038/nature12966.

26. Ofek G, Guenaga FJ, Schief WR, Skinner J, Baker D, Wyatt R, Kwong PD. 2010. Elicitation of structure-specific antibodies by epitope scaffolds. Proc Natl Acad Sci U S A 107:17880–17887. https://doi.org/10.1073/pnas.1004728107.

27. Guenaga J, Dosenovic P, Ofek G, Baker D, Schief WR, Kwong PD, Karlsson Hedestam GB, Wyatt RT. 2011. Heterologous epitope-scaffold prime: boosting immuno-focuses B cell responses to the HIV-1 gp41 2F5 neutralization determinant. PLoS One 6:e16074. https://doi.org/10.1371/journal.pone.0016074.

28. Holm L, Sander C. 1995. Dali: a network tool for protein structure comparison. Trends Biochem Sci 20:478–480. https://doi.org/10.1016/s0968-0004(00)89105-7.

29. Correia BE, Ban YE, Friend DJ, Ellingson K, Xu H, Boni E, Bradley-Hewitt T, Bruhn-Johannsen JF, Stamatatos L, Strong RK, Schief WR. 2011. Computational protein design using flexible backbone remodeling and resurfacing: case studies in structure-based antigen design. J Mol Biol 405:284–297. https://doi.org/10.1016/j.jmb.2010.09.061.

30. Azoitei ML, Ban YE, Julien JP, Bryson S, Schroeter A, Kalyuzhniy O, Porter JR, Adachi Y, Baker D, Pai EF, Schief WR. 2012. Computational design of high-affinity epitope scaffolds by backbone grafting of a linear epitope. J Mol Biol 415:175–192. https://doi.org/10.1016/j.jmb.2011.10.003.

31. Leaver-Fay A, Tyka M, Lewis SM, Lange OF, Thompson J, Jacak R, Kaufman K, Renfrew PD, Smith CA, Sheffler W, Davis IW, Cooper S, Treuille A, Mandell DJ, Richter F, Ban YE, Fleishman SJ, Corn JE, Kim DE, Lyskov S, Berrondo M, Mentzer S, Popovic Z, Havranek JJ, Karanicolas J, Das R, Meiler J, Kortemme T, Gray JJ, Kuhlman B, Baker D, Bradley P. 2011. ROSETTA3: an object-oriented software suite for the simulation and design of macromolecules. Methods Enzymol 487:545–574. https://doi.org/10.1016/B978-0-12-381270-4.00019-6.

32. Fleishman SJ, Leaver-Fay A, Corn JE, Strauch EM, Khare SD, Koga N, Ashworth J, Murphy P, Richter F, Lemmon G, Meiler J, Baker D. 2011. RosettaScripts: a scripting language interface to the Rosetta macromolecular modeling suite. PLoS One 6:e20161. https://doi.org/10.1371/journal.pone.0020161.

33. Sheffler W, Baker D. 2009. RosettaHoles: rapid assessment of protein core packing for structure prediction, refinement, design, and validation. Protein Sci 18:229–239. https://doi.org/10.1002/pro.8.

34. Brune KD, Leneghan DB, Brian IJ, Ishizuka AS, Bachmann MF, Draper SJ, Biswas S, Howarth M. 2016. Plug-and-display: decoration of virus-like particles via isopeptide bonds for modular immunization. Sci Rep 6:19234. https://doi.org/10.1038/srep19234.

35. Thrane S, Janitzek CM, Matondo S, Resende M, Gustavsson T, de Jongh WA, Clemmensen S, Roeffen W, van de Vegte-Bolmer M, van Gemert GJ, Sauerwein R, Schiller JT, Nielsen MA, Theander TG, Salanti A, Sander AF. 2016. Bacterial superglue enables easy development of efficient virus-like particle based vaccines. J Nanobiotechnology 14:30. https://doi.org/10.1186/s12951-016-0181-1.

36. Winter G, Lobley CM, Prince SM. 2013. Decision making in xia2. Acta Crystallogr D Biol Crystallogr 69:1260–1273. https://doi.org/10.1107/S0907444913015308.

37. McCoy AJ, Grosse-Kunstleve RW, Adams PD, Winn MD, Storoni LC, Read RJ. 2007. Phaser crystallographic software. J Appl Crystallogr 40:658–674. https://doi.org/10.1107/S0021889807021206.

38. Bricogne GBE, Brandl M, Flensburg C, Keller P, Paciorek W, Roversi PSA, Smart OS, Vonrhein C, Womack TO. 2017. Buster version 2.10.3. Global Phasing Ltd., Cambridge, United Kingdom.

39. Emsley P, Cowtan K. 2004. Coot: model-building tools for molecular graphics. Acta Crystallogr D Biol Crystallogr 60:2126–2132. https://doi.org/10.1107/S0907444904019158.

40. Fougeroux C, Turner L, Bojesen AM, Lavstsen T, Holst PJ. 2019. Modified MHC class II-associated invariant chain induces increased antibody responses against Plasmodium falciparum antigens after adenoviral vaccination. J Immunol 202:2320–2331. https://doi.org/10.4049/jimmunol.1801210.